Sustainable Cities and Society 35 (2017) 581–593

Contents lists available at ScienceDirect

Sustainable Cities and Society

journal homepage: www.elsevier.com/locate/scs

Retrofitting building roofs with aerodynamic features and solar panels to reduce hurricane damage and enhance eco-friendly energy production

Aly Mousaad Aly*, Chanachock Chokwitthaya, Raymond Poche

Department of Civil Engineering, Louisiana State University, USA

ARTICLE INFO

Keywords:
Aerodynamic loads
Bluff body
Solar panels
CFD
LES
Open-jet testing
Pressure coefficients
Low-rise buildings

ABSTRACT

Wind-induced negative pressure on roofs of low-rise buildings is a major source of losses and community disruption. Vortex suppression technologies may reduce wind loads on buildings; however, it is challenging to implement an effective strategy to reduce wind loads on roofs with minimal loads on the mitigation feature itself. In this paper, the performance of different aerodynamic mitigation features is investigated in a comparative study. The results show that solar panels are relatively effective in reducing wind-induced uplift forces on a flat roof. Compared with all mitigation features presented, the airfoil is the most effective in reducing uplift loads, with promises to proceeding research in this area. In addition, the study investigates wind impact on a gable roof building with different configurations of solar panels, to reduce wind-induced loads on the host building while maintaining a visually appealing installation to permit broad usage and application. Pressure coefficients on roofs and solar panels from both computational fluid dynamics (CFD) simulations and laboratory experiments are compared. The study shows that the optimal roof/solar panel combination reduces wind loads on low-rise buildings, i.e. improves the performance, in addition to providing ecofriendly energy especially when power outage is expected.

1. Introduction

1.1. Background

Wind-induced pressures on low-rise buildings may cause severe and/or sustained loads both of which are detrimental to the structure and put the inhabitants at risk. Windstorms vary from strong winds causing little to moderate damage to extreme winds from hurricanes, tornadoes, or heavy storms causing massive destruction. It is vital to build secure and more efficient infrastructure to balance safety issues with the reality of limited resources (resilience with sustainability). Wind-induced negative pressures develop due to flow separation when high velocity winds pass over the sharp corners of a building (Holmes, 2015). Negative pressures cause uplift effect that can detach panels, tiles, and/or membranes from roofs, like in the case of residential homes or industrial buildings. High suction is usually experienced at the corners of the windward edges (Lin, Surry, & Tieleman, 1995; Mehta, Levitan, Iverson, & McDonald, 1992; Stathopoulos, Baskdran, & Go, 1990; Tieleman, Surry, & Lin, 1994). Negative pressures that develop on roofs of low-rise buildings depend on the shape, among other factors, as a key parameter that affects the pattern and intensity of flow separation and hence wind-induced loads (Gerhardt & Kramer, 1992).

1.2. Aerodynamic mitigation

Wind loads on bluff bodies are dominantly governed by their shapes, among other factors (Davenport 1995). Accordingly, an aerodynamic mitigation approach should rely on shape modification as a technique by which aerodynamic loads can be greatly reduced. The shape of an airplane wing enables flight. It includes slats and flaps, as mechanisms that can be positioned to control aerodynamic forces developed on the plane, and are useful for landing and takeoff (Fig. 1). Turning the leading edge of the slat and the trailing edge of the flap downward increases the lift, while the large aft-projected area of the flap increases the drag, which slows the airplane down for landing. Similar to the way in which the airplane is manipulated for landing, an aerodynamic roof edge may be designed to reduce the total uplift loads on roofs of low-rise buildings. The main objective of a successful aerodynamic mitigation approach is to keep the roof permanently secured by minimizing uplift forces.

Secured roofs under wind loads may reduce windstorm-induced losses. Different roof mitigation strategies are suggested in literature (Banks, Sarkar, Wu, & Meroney, 2001; Bitsuamlak & Warsido, 2012; Blessing, Chowdhury, Lin, & Huang, 2009; Cochran & English, 1997; Kopp, Mans, & Surry, 2005; Lin, Montpellier, Tillman, Riker, & Gx,

* Corresponding author.
E-mail address: aly@lsu.edu (A.M. Aly).

http://dx.doi.org/10.1016/j.scs.2017.09.002
Received 22 October 2016; Received in revised form 1 August 2017; Accepted 1 September 2017
Available online 09 September 2017

Fig. 1. Similar to an airplane landing and takeoff mechanism, aerodynamic features are inspired to reduce wind uplift loads: (a) slats (leading edge), and (b) flaps (trailing edge).

2008; Lin, Montpellier, & Tillman, 2011; Suaris & Irwin, 2010). Six different mitigation devices were tested in (Chowdhury & Blessing, 2007) and the Flat Roof Aero Edge Guard yielded significant decrease in localized negative pressures near roof corners. Experiments on a 1:100 scale Texas Tech University (TTU) test buildings were conducted under multiple flow conditions (Mahmood, Srinivas, & Budair, 2008), showing that rounding the edges of the building may decrease negative pressures. In addition, research carried out by Pindado Carrion et al. (2009) shows that cantilever parapets may reduce uplift forces as they disturb the formation of conical vortices (Banks & Meroney, 2001; Franchini, Pindado, Meseguer, & Sanz-Andrés, 2005; Pindado Carrion, Meseguer Ruiz, Franchini, & Barrero Gil, 2009). Also, screens were employed to suppress the conical roof vortices (Cochran & English, 1997). Additional aerodynamic edges and devices were studied (Banks et al., 2001; Blessing et al., 2009; Suaris & Irwin, 2010). However, a challenge with common architectural features (ex., screens and aerodynamic edges) is that the device may be vulnerable due to exposure to extreme drag and/or lift forces leading to failure with a potential of becoming a windborne debris, leaving the roof unprotected. The mitigation features should be further investigated to ensure that the loads and stresses developed on the mitigation features themselves are within the reasonable and allowable limits. The challenge is on exploring mitigation features that can reduce wind loads, not only at the corners, but also on the entire roof, and create minimal loads on the feature itself. Aerodynamic features with relatively high lift and drag forces may increase the overall wind loads on the main structure, which is not an economic solution. In the current paper, different aerodynamic mitigation techniques and devices were tested computationally in a comparative study to know the best approach for maximum roof protection with minimal loads introduced on the feature. This is an important consideration for the design of the main force resisting system of a low-rise building. In addition, an ideal mitigation feature should be attractive to building owners to permit widespread usage and applicability, which makes the investigations of the potential use of architectural features, such as solar panels, an important consideration.

1.3. Renowned interest in solar energy

The importance of solar energy as a source of eco-friendly energy was documented early in 1911 (Shuman, 1911). With worldwide concerns regarding the impact that combustible fuels have on the increase in greenhouse gas emissions and climate change, sustainable development policies supporting the integration of renewable energies have been implemented. Photovoltaic (PV) solar panels are common devices used for harvesting energy (Singh, 2013), and perhaps technology will lead to '*Covering the Planet with Solar Panels*' (Webb, 2007).

The popularity of the solar panel technology is increasing and spreading across the world and it is especially convenient on buildings as there is no need for power transmission over a long distance (compared to the case of solar farms). The technology provides various advantages such as reducing pollution, acting as a roof heat shield, increasing green energy production, and reducing electrical cost.

However, the wind flow and the aerodynamics of low-rise buildings are quite complicated due to flow separation around the building and other fluid dynamic mechanisms. Therefore, wind-induced loads govern the design and installation of solar panels. Installing solar panels on a building's roof may increase the uplift forces and the over estimation of these forces can significantly increase the construction cost. The design of solar panels on roofs of buildings requires accurate information and the present structural design codes still need more information to be directly applicable to the structural solar systems (Schellenberg, Maffei, Telleen, & Ward, 2013). In addition, there is a limited number of studies that attempt to look at the overall wind loads brought to a building after the solar panels are installed (Kopp, Farquhar, & Morrison, 2012; Stenabaugh, Iida, Kopp, & Karava, 2015). Most of available studies are focused on the estimation of the wind loads on the panels themselves. There is little attention to the overall loads on the host roof after installation.

1.4. CFD as a tool for wind load estimation

Considering the high demand for solar power and the variations among the solar technologies available, several wind tunnel and Computational Fluid Dynamics (CFD) studies exist on the subject of solar panel aerodynamics. CFD is a powerful tool that has been used to carry out and verify research in various engineering fields, especially wind engineering. CFD has plenty of advantages such as the potential to collect continuous flow data and study cases that are challenging to be investigated experimentally (for example, full-scale testing of large structures). In CFD, there is no interference effects of sensors on the aerodynamic loads, which can be an issue in laboratory experiments. In wind tunnel experiments, correct scaling of the flow and the test objects may lead to small models, to obtain similar physics as the case in full-scale. The smaller the model, the fewer measurement sensors can be installed (Aly, 2016; Aly & Bitsuamlak, 2013). These issues and restrictions do not exist in CFD.

CFD has been successfully used for wind load estimation on bluff bodies, for instance, it was employed to achieve optimal tall buildings design (Kareem, Spence, Bernardini, Bobby, & Wei, 2013). Aerodynaic shape optimization was studied by a CFD-enabled Kriging-based approach (Bernardini, Spence, Wei, & Kareem, 2015). Also, aerodynamic shape optimization for corners of tall buildings using CFD was invistigated in detail (Elshaer, Bitsuamlak, & El Damatty, 2015). Iaccarino, Ooi, Durbin, and Behnia, (2003) performed a computational experiment by using the Reynolds Stress Model (RSM) to test a cube in a wind field (Iaccarino et al., 2003). They proved that modelling the flow with the unsteady Reynolds-averaged Navier–Stokes (RANS) equations provides good quantitative and qualitative agreement with experimental data when the flow is not statistically stationary. In contrast, RANS repeatedly produced errors since the method neglects the average

flow component field of the periodic vortex shedding. Janajreh and Simiu (2012) carried out CFD simulations on a small-scale building by Large Eddy Simulation (LES) and compared the results with wind tunnel testing (Janajreh & Simiu, 2012). Their results show that LES provided a notable agreement with the wind tunnel measurements, in terms of mean pressures, but significantly underestimated the peak values of pressures and the turbulent intensity. In addition, there are research papers that attempted to compare RANS with LES. Aboshosha, Elshaer, Bitsuamlak, and El Damatty (2015) presents consistent inflow turbulence generator for LES evaluation of wind-induced responses for tall buildings (Aboshosha et al., 2015).

It is stated by Davenport that the proper selection of inflow boundary conditions leads to a better simulation for wind flow field (Davenport, 1995). Huang, Li, and Wu (2010) suggested the discrete random flow generator (DRFG) method to produce turbulent velocity field that has turbulent spectra close to the target ABL flow characteristics, and Aboshosha et al. (2015) modified the technique to maintain the continuity and the coherency of the inflow in the consistent discrete random flow generator (CDRFG) technique (Aboshosha et al., 2015; Huang et al., 2010). Cheng, Lien, Yee, and Sinclair (2003) compared the results obtained with RANS and LES on a matrix cube model (Cheng et al., 2003). Their results show that both RANS and LES turbulence closures could reasonably predict the main characteristics of the mean flow. However, considering predictions of the flow structure at the leading top and side edges of the cube, along with vortex shedding in the wake and recirculation on the front of the cube, their results showed that LES gave a more accurate estimate than RANS when compared with the experimental data. After comparing the computational results of vortex shading around a bluff body by RANS and LES models, Lakehal and Rodi (1997) discovered that turbulence closures with RSM over-predicted the separation length, when compared with LES that produced a better agreement with the experimental results (Lakehal & Rodi, 1997).

1.5. Focus of the current study

As discussed previously, there are many published research papers dealing with numerous low-rise buildings by CFD and wind tunnel testing, in terms of aerodynamic mitigation and solar panels installed on roofs. However, two important knowledge gaps exist: (1) effect of wind loads on the aerodynamic features themselves, and (2) a lack of understanding of the impact of the solar panels on the overall wind induced loads on the primary structure. To fill these gaps, the current study focuses on aerodynamic features that not only can reduce the wind loads on the roof at its corners, but also can reduce the wind load far from corners and most importantly minimize the loads on the mitigation feature itself. In addition, solar panels on a gable roof building are studied with the objective of understanding their impact on the overall wind-induced loads on the building, with different configurations. CFD with LES is employed in the current paper and the results are validated with wind tunnel and open-jet measurements.

2. Methodology

2.1. Numerical modeling

The software ICEMCFD was used to generate the computational meshes. ANSYS Fluent, a computational fluid dynamic software, was then applied to simulate the computational experiments (Fluent, 2011). Both RANS and LES are employed as turbulence closures. The RSM is one of the most effective turbulence closures in RANS (Vijiapurapu & Cui, 2010). In RSM, Reynolds stresses are solved directly using transport equations, avoiding isotropic viscosity assumption of other models and can be used for vastly swirling flows. The quadratic pressure-strain option improves the performance of simulating many basic shear flows as in the formulae (Fluent, 2011):

$$\begin{aligned}\frac{\partial}{\partial t}(\rho\overline{u_i'u_j'}) + \frac{\partial}{\partial x_k}(\rho u_k\overline{u_i'u_j'}) = &-\frac{\partial}{\partial x_k}[\rho\overline{u_i'u_j'u_k'} + \overline{p(\delta_{kj}u_i' + \delta_{ik}u_j')}] + \frac{\partial}{\partial x_k}\left[\mu\frac{\partial}{\partial x_k}(\overline{u_i'u_j'})\right]\\ &- \rho\left(\overline{u_i'u_j'}\frac{\partial u_j}{\partial x_k} + \overline{u_j'u_k'}\frac{\partial u_i}{\partial x_k}\right) - \rho\beta(g_i\overline{u_j'\theta} + g_j\overline{u_i'\theta})\\ &+ \overline{p\left(\frac{\partial u_i'}{\partial x_j} + \frac{\partial u_j'}{\partial x_i}\right)} - 2\mu\overline{\frac{\partial u_i'}{\partial x_k}\frac{\partial u_j'}{\partial x_k}}\\ &- 2\rho\Omega_k(\overline{u_j'u_m'}\epsilon_{ikm} + \overline{u_i'u_m'}\epsilon_{jkm})\end{aligned} \quad (1)$$

in other words, Local Time Derivative + Convection = − (Turbulent Diffusion + Molecular Diffusion) − Stress Production − Buoyancy Production + Pressure Strain − Dissipation − Product by System Rotation. The term $(\rho\overline{u_i'u_j'})$ is the exact transport equations for the transport of the Reynolds stresses applied to a three dimensional Cartesian coordinate using tensor notation to indicate direction; ϵ is the turbulence dissipation rate; u is the velocity in different directions; g is the gravity force; and β is the coefficient of thermal expansion. RSM gives more accurate predictions for complex flows than the two-equation models (k-ϵ) because it accounts for the effect of streamline curvature, swirl, rotation and rapid changes in strain rate (Salaheldin, Imran, & Chaudhry, 2004; Vijiapurapu and Cui 2010; Wegner et al., 2004; Zhai, Zhang, Zhang, & Chen, 2007). However, there are some limitations to the RSM predictions. The RSM treats both large and small-scale turbulence equally leading to possibly inaccurate results (Janajreh & Simiu, 2012). The current study uses the RSM closure in steady-state simulations as a tool for investigating different mitigation features. The LES turbulence closure is employed for the estimation of wind loads on a gable roof building with solar panels.

LES is one of the most effective turbulence closures used for transient analysis, to estimate peak wind loads (Li & Yu, 2010; Luo, Hinton, Liew, & Tan, 2004; Shur, Spalart, Strelets, & Travin, 2008; Troldborg & Sørensen, 2014). From the continuity equation evaluated at the center of the cell and filtering the incompressible Navier-Stoke equations, the governing equations for LES can be obtained (Fluent, 2011):

$$\text{Continuity equation}\quad \frac{\partial\overline{\rho}}{\partial t} + \frac{\partial\overline{\rho u_i}}{\partial x_i} = 0 \quad (2)$$

$$\text{Filter Navier-stoke equation}\quad \frac{\partial\overline{u_i}}{\partial t} + \frac{\partial}{\partial x_j}(\overline{u_i u_j}) = -\frac{1}{\rho}\frac{\partial\overline{p}}{\partial x_i} + \frac{\partial}{\partial x_j}\left(\nu\frac{\partial\overline{u_i}}{\partial x_j}\right) - \frac{\partial\tau_{ij}}{\partial x_j} \quad (3)$$

$$\text{Sub grid scale turbulent stress}\quad \tau_{ij} = \rho(\overline{u_i u_j} - \overline{u_i}\,\overline{u_j}) \quad (4)$$

where u is the component of the velocity vector; x is the direction of velocity; ρ is the air density; and ν is the kinematic viscosity. The bar represents the filtered Navier-Stokes equation of large-scale terms or resolved scales (grid filtering).

2.2. Aerodynamic features on a flat roof building

Scaled models of a TTU building are used for the case of aerodynamic features on a flat roof. The TTU test building has planar dimensions of 9.1 m × 13.7 m, an eave height of 4 m and a nearly flat roof (Levitan, Mehta, Vann, & Holmes, 1991; Levitan & Mehta, 1992; Mehta et al., 1992). The building is modeled inside a computational domain with length = 17 h, width = 10 h, and height = 5.5 h, where h is the building's height (Fig. 2). Each computational test was run under a wind direction of 45° due to the significance of conical vortices on the roof under such exposure. Aerodynamic mitigation techniques were investigated by implementing aerodynamic devices in the form of parapets, inclined parapets, curved edges, and airfoil edges (Fig. 3) (Aly & Bresowar, 2016). Fig. 4 shows the mesh used for the case of slope-in mitigation feature on the flat roof. A grid independence study was carried out and the results indicated that tetra elements with prismatic layers around all walls is a good choice. Three different values were given for the size of the feature (dimension h as indicated in

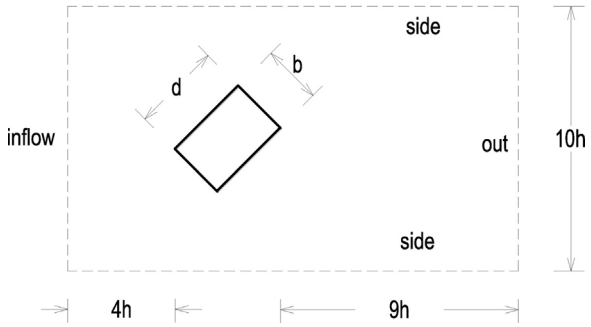

Fig. 2. Computational domain around the flat roof building under wind direction angle of 45°. The building height (h) was used as a parameter for setting the dimensions of the domain. The domain height is 5.5 h.

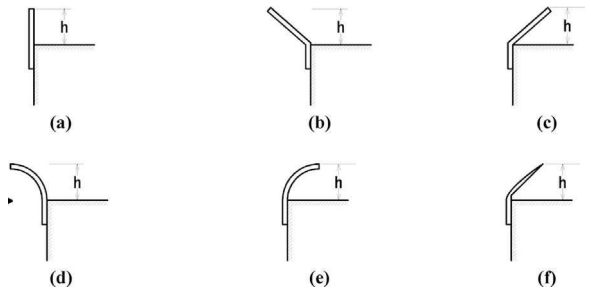

Fig. 3. Roof mitigation devices: (a) parapet; (b) parapet with an outer slope (slope-out); (c) parapet with an inner slope (slope-in); (d) circular device concaved out (circular-out); (e) circular device concaved in (circular-in); and (f) airfoil (half profile) (Aly & Bresowar, 2016).

Table 1
Aerodynamic force coefficients for different mitigation features installed on a flat roof: 18 mitigation scenarios, in addition to the bare roof case.

arrangement	size	building		feature		total	
		C_d	C_l	C_d	C_l	C_d	C_l
bare roof	–	1.02	1.33	–	–	1.02	1.33
a) parapet	small	1.12	1.03	0.23	0.04	1.35	1.07
	medium	1.14	0.99	0.42	0.04	1.56	1.07
	large	1.18	1.26	0.55	0.04	1.73	1.23
b) slope-out	small	1.15	1.06	0.26	0.17	1.41	1.17
	medium	1.18	0.92	0.49	0.30	1.67	1.18
	large	1.29	0.87	0.76	0.40	2.05	1.26
c) slope-in	small	1.04	0.77	0.09	0.13	1.13	1.04
	medium	1.07	0.89	0.23	0.11	1.30	1.03
	large	1.09	1.11	0.29	0.04	1.38	1.19
d) circular-out	small	1.08	1.08	0.25	0.24	1.33	1.28
	medium	1.18	0.98	0.46	0.49	1.64	1.36
	large	1.26	0.90	0.68	0.71	1.94	1.50
e) circular-in	small	1.01	0.62	0.06	0.21	1.07	1.01
	medium	1.05	0.58	0.18	0.31	1.23	1.05
	large	1.06	0.75	0.24	0.39	1.30	1.26
f) airfoil	small	1.03	0.71	0.10	0.12	1.13	0.96
	medium	1.07	0.77	0.22	0.17	1.29	1.01
	large	1.08	1.02	0.27	0.14	1.35	1.20

Fig. 3) and three different simulations were run for every individual mitigation feature. The dimension d and h were set to represent a small size 8%, a medium size 16%, and a large size 24% of the building's height. This led to a total number of simulations of N = (1(bare roof)) + (3(sizes) × 6 (different aerodynamic devices)) = 19, as listed in Table 1.

ICEM CFD was used through the Louisiana State University (LSU)

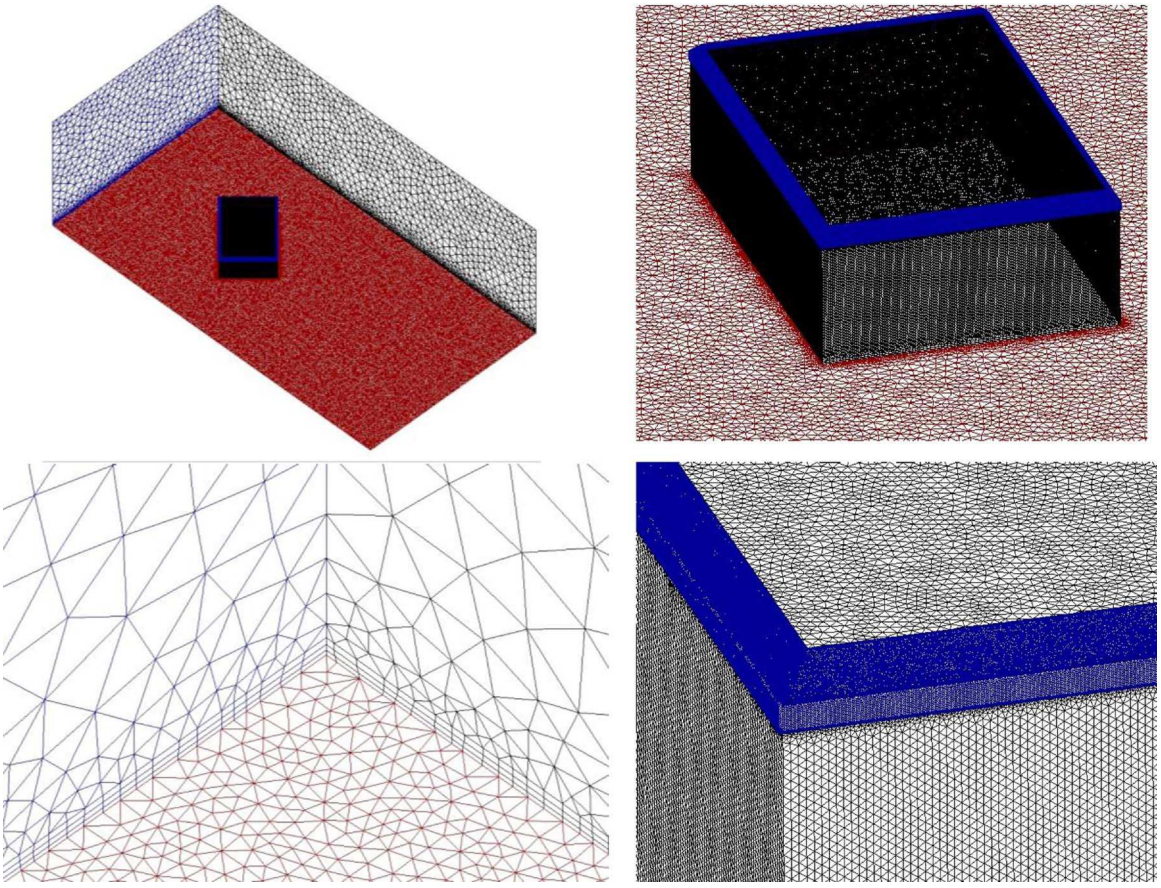

Fig. 4. Mesh of the flat roof building with the slope-in aerodynamic mitigation feature.

virtual lab (HPC, 2017). The computational domain has inlet, outlet, top, ground, and side surfaces. A user defined function was used to provide the mean wind speed and turbulence intensity characteristics of a typical open-terrain exposure at the inlet of the computational domain, for steady simulations with RSM. All walls were assigned to a no slip boundary. The conditions at the sides and top surfaces of the computational domain were assigned to a symmetry boundary condition while the outlet surface was set as outflow. ANSYS FLUENT (Fluent, 2011) was used as the solver and for post-processing. The results from a high-resolution mesh that does not show dependency on the grid size (the grid independence study was carried out by taking into account different grid sizes: coarse, medium and fine) are considered in the comparison among all mitigation techniques and features.

In the current study, the drag and the force coefficients are used as criteria for comparison among different mitigation techniques/features. The drag coefficient of force (C_d) on the building and/or the mitigation feature is defined as follows:

$$C_d = F_d/(0.5\rho U^2 hd) \quad (5)$$

in which F_d is the drag force, ρ is the air density, U is the reference wind speed at the eave height (h) of the building, and d is the length of the building (Fig. 2). Similarly, the lift coefficient of force (C_l) on the building and/or the mitigation feature is defined as follows:

$$C_l = F_l/(0.5\rho U^2 hd) \quad (6)$$

where F_l is the lift force.

2.3. Solar panels on a gable roof building

A bare gable roof and solar panel models were selected to mimic the experimental work of Aly and Bitsuamlak (2014) as shown in Fig. 5 with the dimension of a small-scale (1:15) building model of 27.21 in. (0.691 m) by 47.75 in. (1.213 m), and 11.2 in. (0.285 m) roof mean height with 3:12 roof slope (Aly & Bitsuamlak, 2014). The computational domain for solar panel simulation cases considered a large enough domain to reduce the effects of blockages in the numerical results, and used consistent boundary conditions which were 3d (width) × 15 h (length) × 5 h (height) (Fig. 6). While the flat roof study considered the 45 degrees wind exposure, the gable roof study considered the worst direction angle. This wind direction angle was shown to produce maximum uplift forces as presented in (Aly & Bitsuamlak, 2014). In that study different wind direction angles were considered (from 0° to 350° with an increment of 10°; additional oblique wind directions of 45°, 135°, 225°, and 315° were also tested).

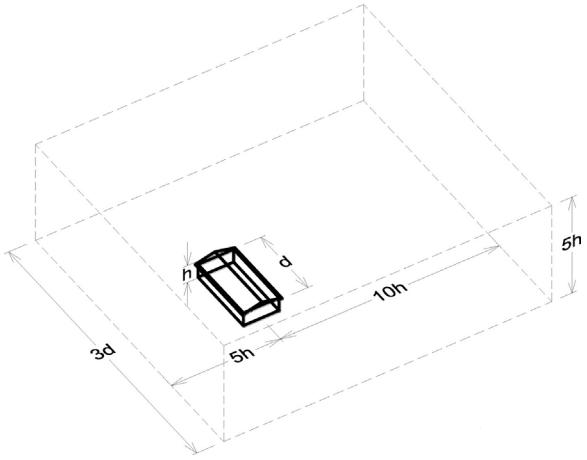

Fig. 6. Schematic representation of the computational domain with the test building (the gable roof case).

For accurate results, the corners, edges, ridges, and solar panels on the roof were assigned with high quality meshes, as illustrated in Fig. 7. The reason for using such expensive type of mesh is the fact that the clearance between the solar panels and the roof and the panels themselves is relatively small that the structured grid was found to be the best option to control the size and number of elements in such small spaces. This was an objective for the accurate simulation of the wind flow underneath the roof-mounted solar panels. An open terrain power law ($\alpha = 0.15$) wind speed profile with a mean wind speed of 17.8 m/s measured at 10 m from the ground in full-scale was used at the inlet. A pressure outlet with a zero-pressure gradient was established. The top and sides of the domain were assigned as a symmetry boundary condition. The building and the solar panels were assigned wall (no slip) boundary condition.

2.4. Convergence of the solution

To ascertain that the CFD solution approaches the exact solution of

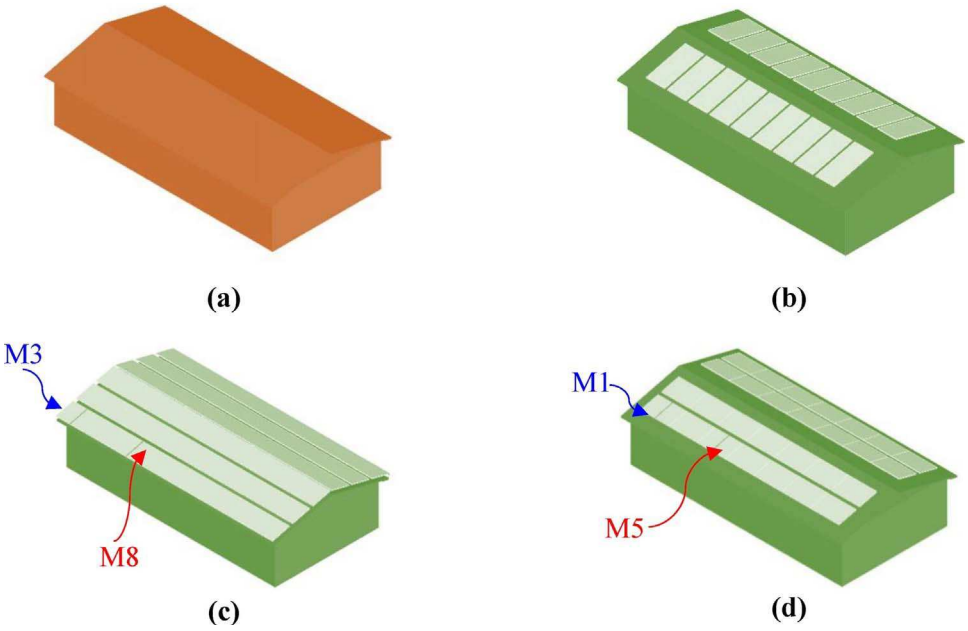

Fig. 5. Different solar panel arrangements were used in the CFD simulations of a gable roof building: (a) bare roof, (b) vertical configuration V2, (c) horizontal configuration H1, and (d) horizontal configuration H2.

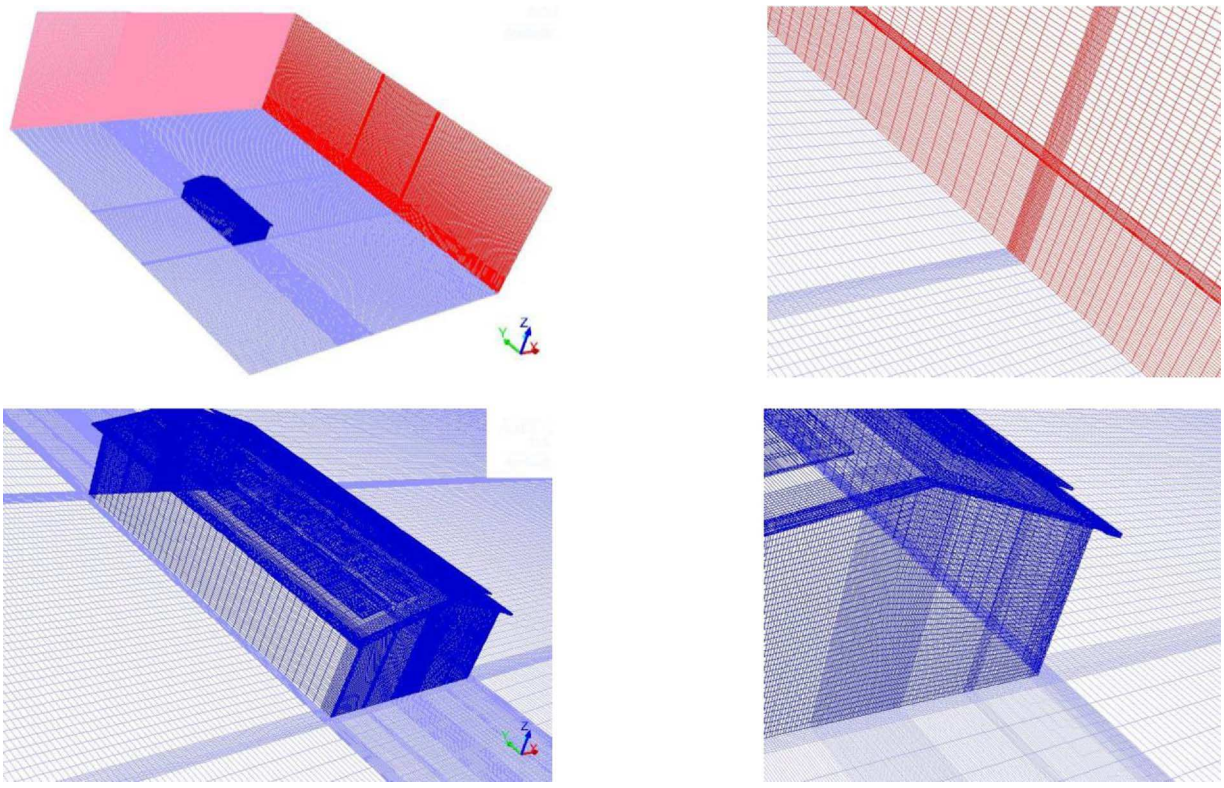

Fig. 7. 3D structured mesh (hexahedral elements) of a gable roof building with solar panels (configuration H2 as designated in Fig. 5).

the governing partial differential equations (PDE), convergence is the most important calculation term. The indirect consideration of convergence needs to be implicated in terms of consistency and stability. For consistency, the formulation of the CFD system should be uniform with the original PDE. For any numerical method to be consistent, the truncation error must become zero when the time step approaches zero. Stability is part of the platform, with the consistency criterion, to ensure convergence. Above all, stability is about increasing or decreasing errors during the calculation (Tu, Yeoh, & Liu, 2009).

For transient analysis with LES, a necessary condition for the convergence of a numerical method for partial differential equations is the numerical/mathematical domain of dependence. This condition is known as the Courant-Friedrichs-Lewy (CFL) or Courant number. The Courant number can indicate how the fluid is moving through the computational cells. If the Courant number is less than or equal to 1, fluid particles move from one cell to another within one time step. If CFL is more than 1, fluid particles move through two or more cells at each time step, which can negatively affect the convergence and accuracy of transient simulations. To indicate the convergence and accuracy of the simulation with LES, the CFL should be less than 1 (Venkatachari, Cheng, Soni, & Chang, 2008). The Courant number is the dimensionless transport per time step. The CFL condition required for stability is (Janajreh & Simiu, 2012):

$$\mathrm{CFL} \equiv \frac{\Delta t.\ V_H}{\min(dx,dy,dz)} < 1 \tag{7}$$

where Δt is the time step (s); V_H is the local flow speed (m/s); and dx, dy and dz are the cell dimensions (m).

As mentioned in the formulae, the Courant number or CFL is calculated based on velocity, cell-size, and the time step at each cell. However, when reducing the grid size, the time step also needs to be reduced to keep the Courant number less than 1, as indicated in the formulae (Wang, Dai, Li, & Zhou, 2012).

The solutions also need to be independent of the mesh resolution. Not checking this is a common cause of erroneous results in CFD, and this process should at least be carried out once for each type of calculation. Having run a simulation on a sequence of grids and found the same results for each grid, the solution is considered grid-convergent. The converged solution is therefore independent of the size of the grid used.

A grid convergence approach was carried out to verify the independence of the models. Two additional coarser grids (medium and coarse grid) of the bare gable roof were created. The element number of very fine, fine, medium, and coarse grids are around 19 million, 16 million, 12 million, and 8 million, respectively. These grids were analyzed and compared in the absolute values of the mean pressure coefficients on the roof in windward direction. The differences of pressure coefficients between those grids were calculated and plotted. Pressure coefficients on the solar panels of each model were analyzed and verified with available experimental results (Aly & Bitsuamlak, 2014).

At the end of each solver iteration, the residual sums for each of the conserved variables are computed. During the numerical procedure, the imbalances (errors) of the discretized equations are monitored and these defects are commonly referred to as the residuals of the system of algebraic equations that measure the extent of imbalances arising from these equations and terminate the numerical process when a specified tolerance is reached. In an iterative numerical solution, the residual will never be exactly zero. However, the lower the residual value is, the more numerically accurate the solution. For satisfactory convergence, the residuals should diminish as the numerical process progresses (Tu et al., 2009). The Semi-Implicit Method for Pressure-Linked Equations (SIMPLE) is a pressure based algorithm solver that was used with the RSM model in this paper. For the LES model, the Pressure Implicit with Splitting of Operator (PISO) scheme solution method was employed.

2.5. Laboratory experimental method

For partial validation of the CFD results of the current study, two types of experimental test results were used: (1) available results from pressures collected on solar panels mounted on a gable roof

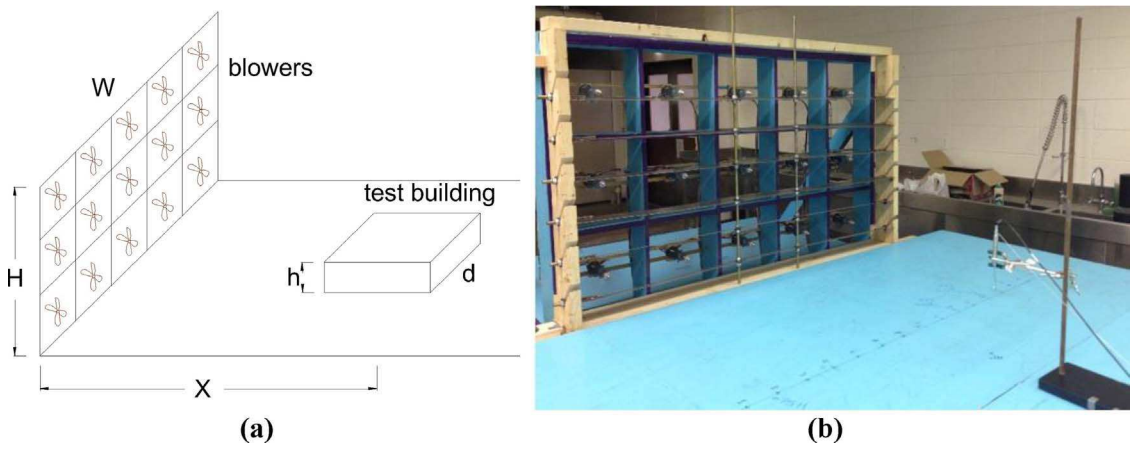

Fig. 8. Open-jet testing: (a) main concept of the open-jet testing – the test model's height (h), width (d), and its location from the exit of the blowers (distance x) are important parameters that depend dominantly on the height (H) and width (W) of the open-jet flow field; (b) picture of a small-scale open-jet simulator at LSU.

(Aly & Bitsuamlak, 2014); and (2) time histories of wind pressures on a bare gable roof obtained by open-jet testing.

The open-jet simulator is a tool for large-scale testing, such as Post-disaster investigation of areas affected by severe winds, and has been useful for understanding the performance of structures under extreme events. The challenges of working with open-jet simulators are the characteristics of wind, the mean wind velocity profile, the turbulent intensities, and scale of the turbulence, which have to be able to accurately represent the atmospheric boundary layers (ABL) wind flow in the desired terrain roughness (Aly, 2014). Fig. 8(a) shows the main concept of open-jet testing. The test model's height (h) and its location from the exit of the blowers (distance x) are important parameters that depend dominantly on the height of the open-jet (H). The distance (x) should be optimized to balance between relatively high wind speed, and a fully developed profile. In addition, the test model's height (h) should be within 20% to one third of the wind field height (H) to allow for realistic pressures on roofs (Aly, Chowdhury, & Bitsuamlak, 2011). The width of the test model is another important parameter (Gol Zaroudi & Aly, 2017). Fig. 8(b) shows a photograph of a small-scale open-jet simulator at LSU. An open-jet hurricane testing facility was recently built at LSU (Aly & Gol-Zaroudi, 2017), where CFD simulations were performed to help reduce the experimental effort by allowing for verifications of several arrangements of flow management schemes. The objective of the CFD simulations was to generate wind profiles with a power law profile that mimic open terrain (power law exponent $\alpha = 0.15$) by examining certain plank setups (inclination angles). The results of the CFD simulation were analyzed as velocity profiles at specific measuring points and that led to a final acceptable arrangement for generating open terrain mean velocity and turbulence intensity profiles (Aly & Gol-Zaroudi, 2017).

Wind velocity data were collected at an optimal test location that was determined by pressure validation and comparison with wind tunnel results (Gol Zaroudi & Aly, 2017). The measurement locations are designated in Fig. 9. The wind profiles of experiment, and target open terrain are plotted and compared with a theoretical target profile as shown in Fig. 10. A scale 1:30 test model of the gable roof building mentioned in Section 2.3 was built for open-jet testing. The building was made from acrylic sheets connected by powerful glue. Pressure sensors were installed with taps distributed on the roof. The experimental setup and the pressure taps layout are shown in Fig. 11. Short tubes were used to carry wind pressures and connect them to pressure transducers. The length of each tube is about 0.2 *m* centimeters because it needed to be short enough so the pressure signal would not be distorted due to distance traveled in the tubes.

Transient pressures and wind velocities for several experiments were collected. The pressure data was collected using ZOC pressure

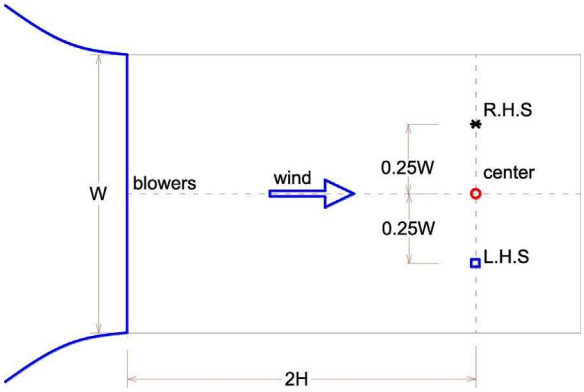

Fig. 9. Location of velocity measurements for open-jet testing.

transducers and RAD 4000 provided by Scanivalve (Scanivalve, 2016). The data was collected at a rate of 625 Hz for a duration of 5 min. To collect 5 min of pressure data, the data rate has to be calculated and taken as the input in setting up the Scantel software, as explained in the following equation (Scanivalve, 2016):

$$\text{data rate} = \frac{1}{\text{period}\times\text{channel}\times\text{AVG}} \tag{8}$$

where the data rate is expressed in Hertz per channel; the period is in microseconds; 'channel' is the number of channels; and AVG is the average term for that scan group. Two cobra probes were used to measure the wind velocity before and during the pressure measuring experiment. The collected data were analyzed by MATLAB software and compared with the CFD LES results, which will be discussed in Section 4.

3. Results from the flat roof building with architectural features

Fig. 12 shows the mean values of the pressure coefficient distribution on a flat roof with the k-e and RSM turbulence closures. While the two models gave the same values for the overall lift coefficient, the RSM model accurately displays the pressure distribution from the influence of the conical vortices. Experimental validation of the CFD results on the bare flat roof building was conducted in (Aly & Bresowar, 2016). For this reason, the RSM turbulence closure was used for investigating the impact of the installation of all features on the overall wind loads on the building. In addition to the bare roof case (no mitigation), Table 1 lists the force coefficients on the entire building and the mitigation devices proposed for 18 different cases. Since the mitigation device will be attached to previously erected structures, it is important to evaluate the load placed on the devices. Table 1 lists the values of the drag and

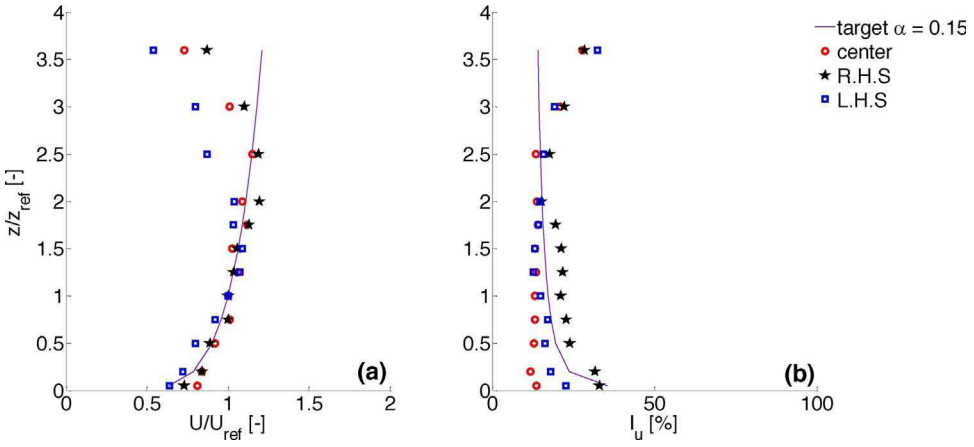

Fig. 10. Wind velocity (a) and turbulence intensity (b) profiles at 2H from the exit of the blowers: the location of the measurements is designated in Fig. 9.

lift force coefficients for each mitigation device. The ideal device would have minimal drag and lift coefficients, which would result in a smaller chance of damage by wind. Five different mitigation devices termed parapet, slope-out, slope-in, circular-out, circular-in, and airfoil were investigated (Fig. 3). Each mitigation device was considered at three different sizes: small (8% of building's height), medium (16% of roof's height) and large (24% of roof's height).

Table 2 lists percentages of reduction/increase in lift and drag force coefficients obtained after the devices were installed. The results show that slope-out and circular-out devices are not significantly effective, compared with the other mitigation devices. Both devices have large drag forces, which brings additional loads to the original building. In addition, the circular-out device can lead to increased uplift forces at both medium and large sizes. Generally, the larger the mitigation device, the larger the drag force produced on the device, leading to increased total drag force that the primary building has to resist. At a certain size, the parapet will bring the heights drag force, compared to slope-in, circular-in and airfoil features. The three devices can bring significant reduction in the total uplift forces produced on the structure ranging from 20% to 28% at small sizes. Changing the shape of the device from slope-in to circular-in or airfoil brings an additional reduction in the roof's uplift force with the cost of increased drag force on the mitigation device. Compared to the slope-in and the circular-in, the airfoil yields the maximum reduction in the total uplift forces produced on both the building and the mitigation feature. This gives promise to proceeding research in this area, especially studies that focus on the shape, size and orientation of the mitigation feature. The slope in device is recommended for manufacturing purposes because of its simpler geometry. In fact, this feature can be a solar panel, for both wind load reduction and eco-friendly energy production.

4. Results from the gable roof building with solar panels

The 8 million-element grid was initially brought into the numerical analysis to investigate the pressure coefficient on the bare roof model and to plot the pressure coefficient contour. The contour plot on the middle of the roof did not show the development of suction pressure coefficients because the grid was not fine enough to catch potential flow separation at the top, corners, and edges of the roof as shown in Fig. 13(d). Next, the number of grid elements was increased to 12 million and 16 million and the simulation was run for 6000 iterations (steady RSM). The result shows some improvement of the pressure coefficients at the top, corners, and edges of the roof but it was still not good enough to be acceptable compared to the experimental data in Ref. Aly and Bitsuamlak (2014). From the previous results, it was obvious that the model still has to be improved in terms of the number of grid elements, in order to obtain the corrected pressure coefficients. Afterward, the 19 million-element grid model was developed and recomputed with the same experiment method to see if the pressure coefficients were improved with 7000 iterations. The result of contour plot in Fig. 13(a) showed high development of mean pressure coefficients on the top, corners, and edges of the roof and it seems to match the laboratory experimental contour plot in (Aly & Bitsuamlak, 2014). From the results of the 19 million-element grid model, i.e., grid independence comparisons between 19 m, 16 m, 12 m, and 8 m elements (Fig. 13) showed that the 19 million-element could represent the grid convergence. This said both grid independence and validation with available wind tunnel results are achieved.

Statistical analysis of extreme values was used to analyze time history data for the 95-percentile case. A contour plot of minimum pressure coefficient (Cpmin) as shown in Figs. 14 and 15 compares the CFD

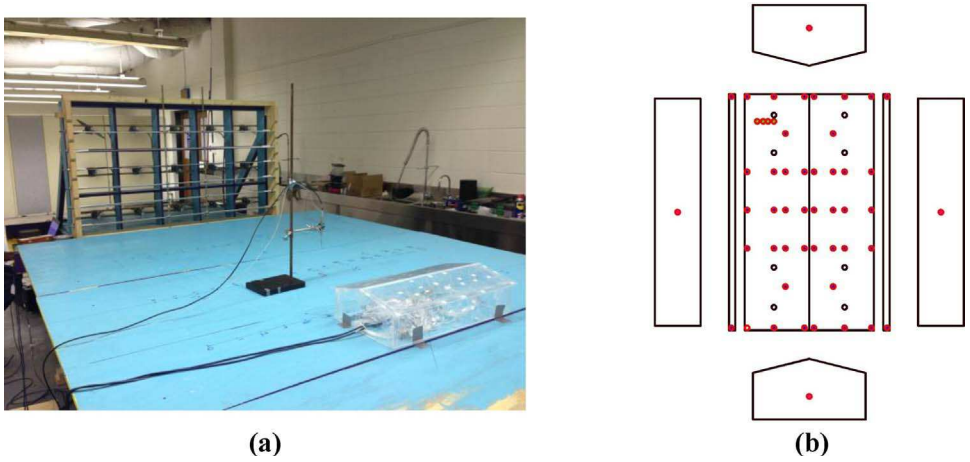

Fig. 11. 1:30 scale model: (a) experimental setup, and (b) pressure tap layout.

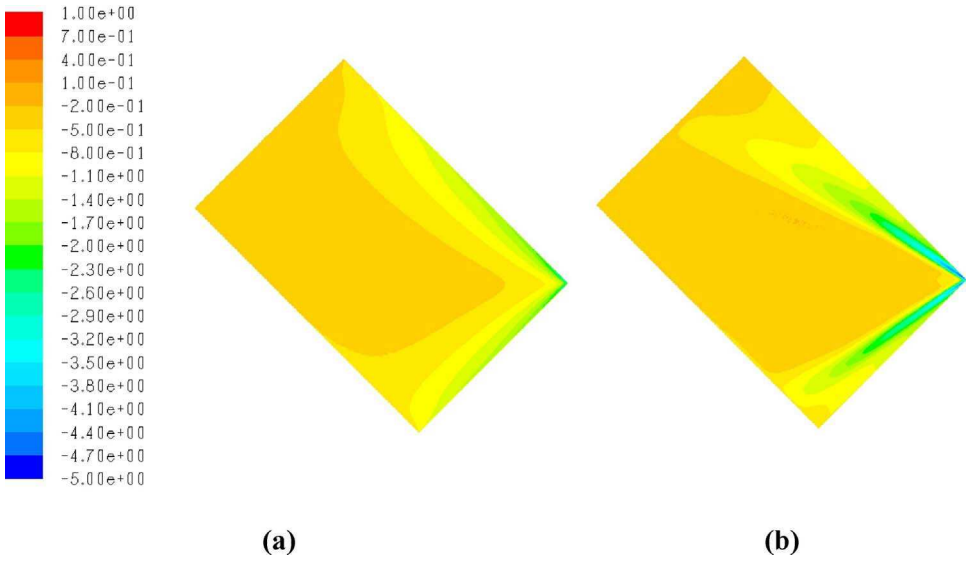

Fig. 12. Mean pressure coefficient distribution on a flat roof: (a) with k-e turbulence closure (Cl = 1.33); and (b) with RSM turbulence closure (Cl = 1.33) (Aly & Bresowar, 2016).

Table 2
Percentages of reduction/increase in the aerodynamic force coefficients of different mitigation features installed on a flat roof.

arrangement	size	building		total	
		C_d	C_l	C_d	C_l
	small	5.7	−22.6	27.4	−19.4
a) parapet	medium	7.5	−25.6	47.2	−19.3
	large	11.3	−5.3	63.2	−7.9
	small	8.5	−20.3	33.0	−12.0
b) slope-out	medium	11.3	−30.8	57.5	−11.0
	large	21.7	−34.6	93.4	−5.0
	small	−1.9	−42.1	6.6	−22.0
c) slope-in	medium	0.9	−33.1	22.6	−22.2
	large	2.8	−16.5	30.2	−10.5
	small	1.9	−18.8	25.5	−3.9
d) circular-out	medium	11.3	−26.3	54.7	2.2
	large	18.9	−32.3	83.0	12.5
	small	−4.7	−53.4	0.9	−24.1
e) circular-in	medium	−0.9	−56.4	16.0	−21.3
	large	0.0	−43.6	22.6	−5.1
	small	−2.8	−46.6	6.6	−27.9
f) airfoil	medium	0.9	−42.1	21.7	−24.1
	large	1.9	−23.3	27.4	−10.0

and experimental data. The results show that most of the pressure coefficients matched between both cases but some positions show disagreements, especially at the edges of the roof. The disagreements may be from some limitation, namely insufficient amount of pressure taps that could not cover the whole roof area.

Fig. 16 shows contour plot of pressure coefficients obtained by CFD, on a gable roof building, with solar panels installed in configuration H2 as shown in Fig. 5. The comparisons of drag and lift coefficients are shown in Table 3 for three different configurations of solar panels, along with the bare roof case. From the results, the uplift force on the primary building is reduced after installing the solar panels. In contrast, the drag coefficient increased after installing the solar panels, but with less significance compared to the reduction in the uplift forces. Overall, this indicates that solar panels can reduce uplift forces on the roof and may produce positive impact on the whole structure, especially low-rise buildings. Table 3 also shows that configuration H2 (see Fig. 5) is the most effective in reducing wind-induced forces on the entire structure. The comparisons of experimental and CFD results shows relative agreement and the results are plotted in Figs. 17 and 18. Fig. 18 shows that configuration H2 reduced the pressure coefficient on the top surface of solar panels since the solar panels are in a position away from the edge and corners of the roof. However, the pressure coefficient underneath the solar panel was increased, possibly due to significant localized wind acceleration underneath the modules. These CFD findings are in agreement with published experimental results

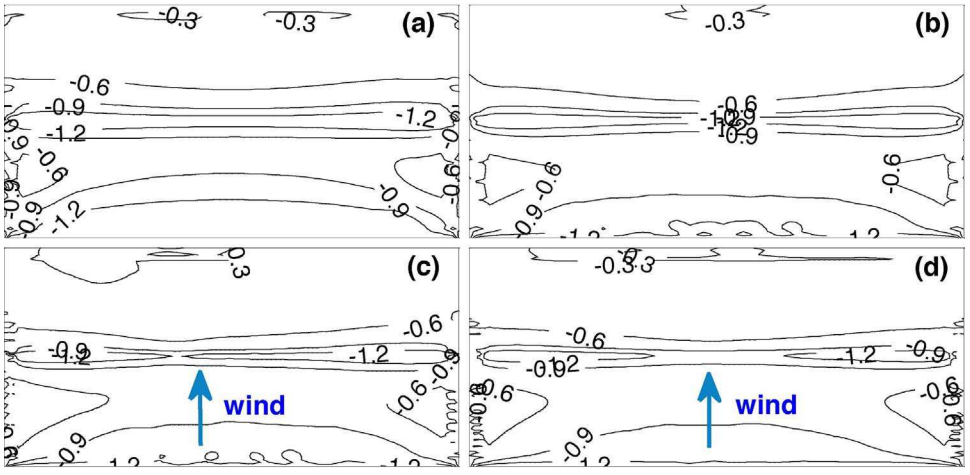

Fig. 13. CFD grid independence study of the gable roof building; mean values of pressure coefficients for serval grids: (a) 19 million-element grid, (b) 16 million-element grid, (c) 12 million-element grid, and (d) 8 million-element grid.

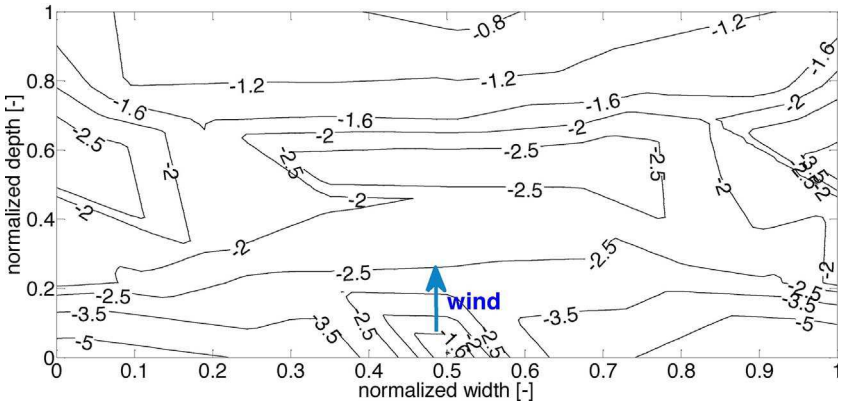

Fig. 14. Contour plot of experimentally obtained (by open-jet testing) minimum pressure coefficient on the gable roof (95 quantile).

(Aly & Bitsuamlak, 2014) that shows that locations of solar panels should be away from the corners and edges of the roof in order to reduce the overall wind uplift loads on the panels themselves. However, the current study shows the potential of the installation of solar panels on roofs, for not only minimizing wind loads on the panels themselves, but also reducing the loads on the entire structure.

5. Discussion

The study presented in the current paper addresses the reduction of wind-induced suctions (a result of flow separation) on flat and gable roofs of low-rise buildings, to reduce potential damage and to allow for economic design. In order to reduce uplift loads on a roof, flow separation should be reduced. This can be achieved by retrofitting the roofs by certain architectural features/devices. The challenge, however, is on exploring mitigation features that can reduce wind loads on not only the corners, but also the entire roof, and create minimal loads on the feature itself, not to become wind-borne debris, or bring significant drag forces to the host building, which is not an economic solution. Different aerodynamic mitigation techniques and devices proposed were tested computationally in a comparative study to help choose the best approach for maximum roof protection with minimal loads introduced on the feature. The results show that a slope-in feature, which can be replaced by solar panels for green energy production, is relatively effective in reducing wind-induced suctions. Such feature, among other devices, can be used for potential roof protection forming economic and green buildings. Future research will focus on the reduction of peak pressures, which will require large eddy simulations for the computational model. In addition, open-jet testing is planned to validate and complement the CFD simulations. The slope-in and the airfoil were placed at a 45° inclination angle. Optimization studies to find the best inclination angle are recommended as future research. The wind direction angle of 45° was chosen as a potential worst-case scenario for wind pressures on the flat roof case. Different wind direction angles need to be considered in the experimental follow up study.

The current study focused on different mitigation features and solar panel arrangements, in a comparative study. That all features on the flat roof where given same height and their aerodynamic performance in terms of reducing wind-induced loads on the host building was investigated. While this comparative study is useful to identify some mitigation features with promises to reduce uplift loads, an optimization approach is recommended, which can be time and resource consuming task, especially when a turbulence closure like LES is employed. The literature has some attempts to use the CFD for reaching the global optimal mitigation shape, by integrating the wind load assessment method with optimization algorithms, to investigate a wider search space (Bernardini et al., 2015; Elshaer et al., 2015; Kareem et al., 2013).

Developing aerodynamic mitigation techniques for roofs of low-rise buildings can bring important solutions in the area of disaster prevention and preparedness, such as taking into account structural safety with affordability and availability. These outcomes would greatly impact the way we design for hurricanes with extreme wind loads and would provide an affordable methodology, which can be used in improving the aerodynamic mitigation techniques for low-rise structures. The main objective of the project of optimizing roof shapes of low-rise buildings, considering aerodynamic mitigation features inspired by the aeronautical industry, and adopting energy-saving modules attached on the surface is new in the construction industry. Securing such devices, such that they would not become a source of debris, is a challenge, which should be addressed carefully. The research and development imperative, with respect to aerodynamic roof mitigation, can help prevent future hazards from becoming disasters. The aim is to protect homeowners, businesses, and communities by the implementation of innovative aerodynamic mitigation solutions that can enhance the resilience and sustainability of the infrastructure, hence more sustainable cities and society.

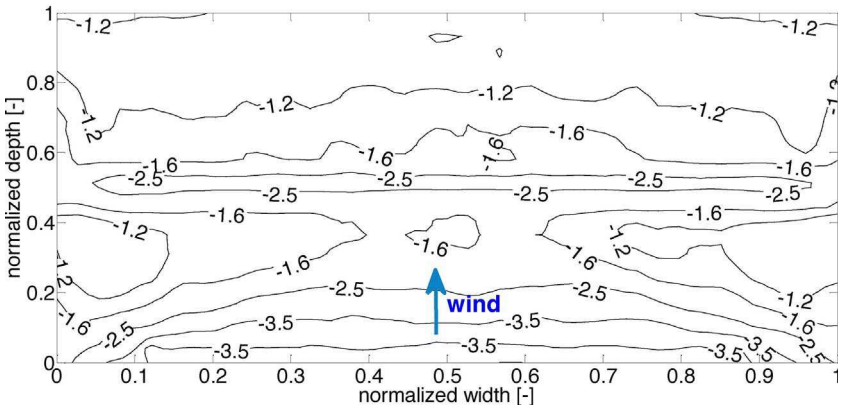

Fig. 15. Contour plot of LES minimum pressure coefficient on the gable roof (95 quantile).

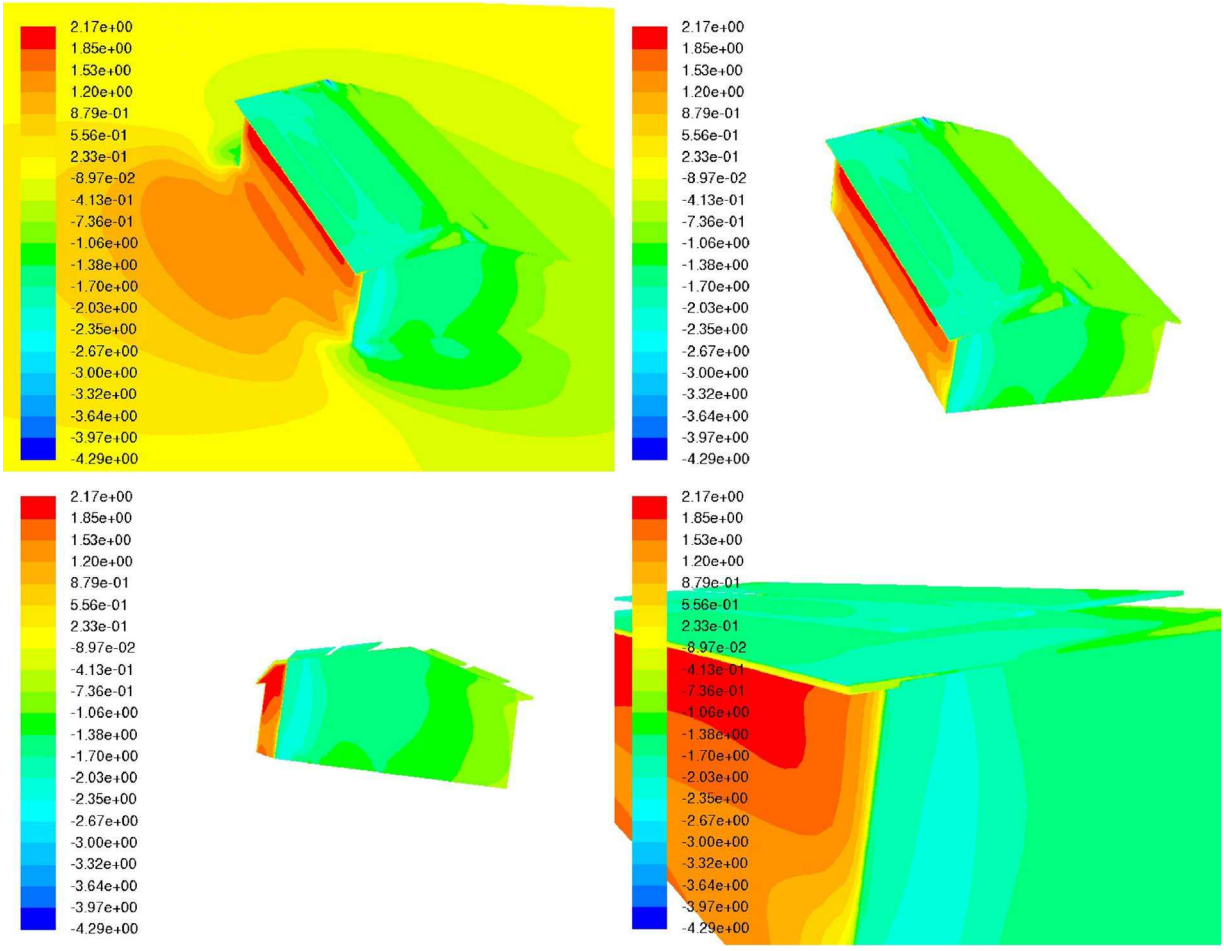

Fig. 16. CFD contour plot of pressure coefficient on the gable roof building with solar panels (configuration H2 as designated in Fig. 5).

Table 3
Drag and lift coefficients for a gable roof building with solar panels at different arrangements (Fig. 5).

arrangement	building		panels		total	
	Cd	Cl	Cd	Cl	Cd	Cl
bare roof	0.449	1.694	0	0	0.449	1.694
H1	0.583	1.132	0.076	−0.010	0.659	1.122
H2	0.625	1.379	0.069	−0.245	0.694	1.134
V2	0.558	1.401	0.037	−0.083	0.595	1.318

6. Conclusion

The study presented in the current paper attempts to compare the performance of aerodynamic roof mitigation features in the reduction of roof suctions produced by high-speed winds on low-rise buildings. Several roof mitigation features were proposed and tested by CFD simulations. For a building with a flat roof, different mitigation devices, including parapets, circular edges, inclined edges, and airfoil edges were investigated. The paper focuses on exploring mitigation devices that not only can reduce loads on the roofs, but also have minimum drag and lift forces on the device itself. In addition, different

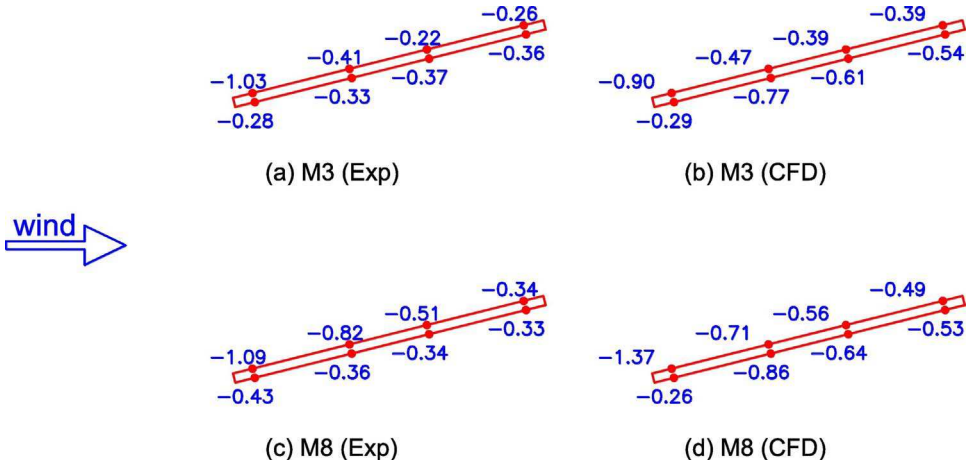

Fig. 17. Comparison between CFD and experimental results of pressure coefficients for configuration H1: modules M3 and M8 are designated in Fig. 5(c).

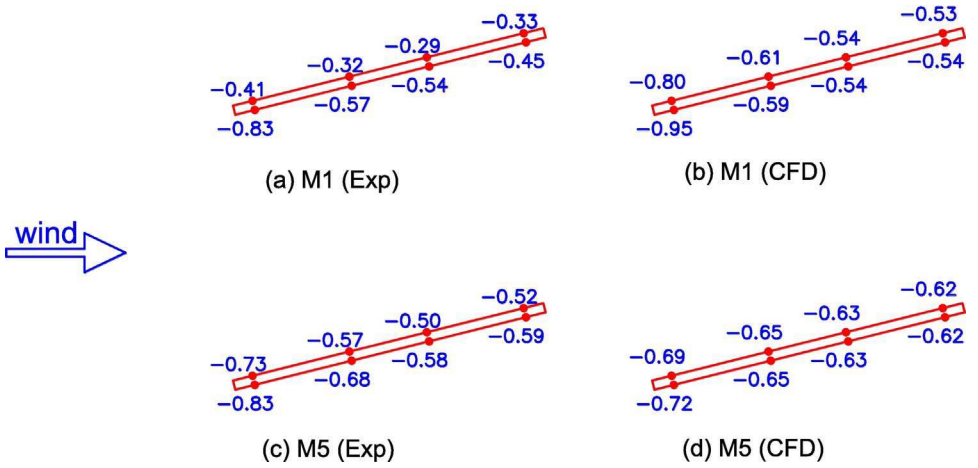

Fig. 18. Comparison between CFD and experimental results of pressure coefficients for configuration H2: modules M1 and M5 are designated in Fig. 5(d).

configurations of solar panels mounted on a gable roof building were investigated, to explore the potential of overall wind uplift reduction to the host building. The contributions of the current paper can be summarized as follows:

- The addition of aerodynamic features to flat roofs of low-rise buildings can bring significant reduction to the uplift force. Depending on the shape and size of the mitigation feature, reduction in the total uplift force on buildings can be substantial with minimal drag forces on the device.
- Aerodynamic features including slope-in, circular-in, parapets, and airfoils can bring significant uplift reductions to the whole structure (roof + device) ranging between 20% and 28%.
- Compared to all mitigation features presented in the current study, the airfoil is shown to produce the lowest uplift loads on the whole structure (roof + feature). This shows promises to proceeding research in this area: shape, size and orientation of the mitigation feature.
- The simple shape of the slope-in mitigation feature makes it attractive for uplift reduction on flat roofs with minimal drag forces on the feature. In fact, the slope-in features initiated an idea to be replaced by solar panels.
- Installing solar panels on buildings with gable roofs allows for various benefits to the building: they can help reduce wind uplift forces when properly arranged, in addition to the obvious benefits of providing ecofriendly energy, especially at a time where power outage is expected (for instance, after windstorms).
- The CFD findings are in agreement with published experimental results (Aly & Bitsuamlak, 2014) that shows that locations of solar panels should be away from the corners and edges of the roof in order to reduce the overall wind uplift loads on the panels themselves. However, the current study shows the potential of the installation of solar panels on roofs, for not only minimizing wind loads on the panels themselves, but also reducing the loads on the entire structure.
- CFD is showing potential benefits; as its results are accurate when careful setup with sufficient number of grid elements (high resolution with structured grid), is followed and a proper turbulence closure is used. In addition, the CFD provides continuous flow information compared to a typical pressure measurement experiment, which is useful for wind load estimation on small size architectural features.

Acknowledgments

The Louisiana Board of Regents supported this research (Research Competitiveness Subprogram – RCS Contract # LEQSF(2016-19)-RD-A-02). Partial support was received from the Gulf of Mexico Alliance (GOMA) (Gulf Star Program Contract # G-121624-00). Financial support was received from the National Science Foundation (NSF Award No. 1361908), to attend a Planning Grant meeting (I/UCRC for Windstorm Hazard Mitigation), and to present the results of this study. The High Performance Computing (HPC) facilities at Louisiana State Ubiversity were used in the current study.

References

Aboshosha, H., Elshaer, A., Bitsuamlak, G. T., & El Damatty, A. (2015). Consistent inflow turbulence generator for LES evaluation of wind-induced responses for tall buildings. *Journal of Wind Engineering and Industrial Aerodynamics, 142*, 198–216.

Aly, A. M., & Bitsuamlak, G. (2013). Aerodynamics of ground-mounted solar panels: Test model scale effects. *Journal of Wind Engineering and Industrial Aerodynamics, 123*, 250–260.

Aly, A. M., & Bitsuamlak, G. (2014). Wind-induced pressures on solar panels mounted on residential homes. *Journal of Architectural Engineering, 20*(1).

Aly, A. M., & Bresowar, J. (2016). Aerodynamic mitigation of wind-induced uplift forces on low-rise buildings: A comparative study. *Journal of Building Engineering, 5*, 267–276.

Aly, A. M., & Gol-Zaroudi, H. (2017). Atmospheric boundary layer simulation in a new open-jet facility at LSU: CFD and experimental investigations. *Measurement, 110*, 121–133.

Aly, A. M., Chowdhury, A. G., & Bitsuamlak, G. (2011). Wind profile management and blockage assessment for a new 12-fan Wall of Wind facility at FIU. *Wind and Structures An International Journal, 14*(4).

Aly, A. M. (2014). Atmospheric boundary-layer simulation for the built environment: Past, present and future. *Building and Environment, 75*, 206–221.

Aly, A. M. (2016). On the evaluation of wind loads on solar panels: The scale issue. *Solar Energy, 135*, 423–434.

Banks, D., & Meroney, R. N. (2001). A model of roof-top surface pressures produced by conical vortices: Model development. *Wind and Structures, 4*(3), 227–246 Techno Press.

Banks, D., Sarkar, P. P., Wu, F., & Meroney, R. N. (2001). A device to mitigate vortex induced rooftop suction. *Americas conference on wind engineering*, 1–10.

Bernardini, E., Spence, S. M. J., Wei, D., & Kareem, A. (2015). Aerodynamic shape optimization of civil structures: A CFD-enabled Kriging-based approach. *Journal of Wind Engineering and Industrial Aerodynamics, 144*, 154–164.

Bitsuamlak, G., & Warsido, W. (2012). Aerodynamic mitigation of roof and wall corner suctions using simple architectural elements. *Journal of Engineering Mechanics*, 396–408.

Blessing, C., Chowdhury, A. G., Lin, J., & Huang, P. (2009). Full-scale validation of vortex suppression techniques for mitigation of roof uplift. *Engineering Structures, 31*(12), 2936–2946.

Cheng, Y., Lien, F. S., Yee, E., & Sinclair, R. (2003). A comparison of large Eddy simulations with a standard k-e Reynolds-averaged Navier-Stokes model for the prediction of a fully developed turbulent flow over a matrix of cubes. *Journal of Wind Engineering and Industrial Aerodynamics, 91*(11), 1301–1328.

Chowdhury, A. G., & Blessing, C. (2007). *Mitigation of roof uplift through vortex suppression techniques.* The International Hurricane Research Center Florida International University.

Cochran, L. S., & English, E. C. (1997). Reduction of roof wind loads by architectural features. *Architectural Science Review, 40*(3), 79–87 Taylor & Francis.

Davenport, A. G. (1995). How can we simplify and generalize wind loads? *Journal of Wind Engineering and Industrial Aerodynamics, 54–55*, 657–669.

Elshaer, A., Bitsuamlak, G., & El Damatty, A. (2015). Aerodynamic shape optimization for corners of tall buildings using CFD. *14th international conference on wind engineering (ICWE)*.

Fluent, A. (2011). *ANSYS Fluent 14.0 user's guide.* Ansys Inc.
Franchini, S., Pindado, S., Meseguer, J., & Sanz-Andrés, A. (2005). A parametric, experimental analysis of conical vortices on curved roofs of low-rise buildings. *Journal of Wind Engineering and Industrial Aerodynamics, 93*(8), 639–650 Elsevier.
Gerhardt, H. J., & Kramer, C. (1992). Effect of building geometry on roof windloading. *Journal of Wind Engineering and Industrial Aerodynamics, 43*(1–3), 1765–1773 Elsevier.
Gol Zaroudi, H., & Aly, A. M. (2017). Open-jet boundary-layer processes for aerodynamic testing of low-rise buildings. *Wind and Structures, 25*(3), http://dx.doi.org/10.12989/was.2017.25.3.000 in press.
HPC (2017). *High Performance Computing (HPC).* Louisiana State University. 7 July, 2017 http://www.hpc.lsu.edu/.
Holmes, J. D. (2015). *Wind loading of structures.* New York: Taylor and Francis.
Huang, S. H., Li, Q. S., & Wu, J. R. (2010). A general inflow turbulence generator for large eddy simulation. *Journal of Wind Engineering and Industrial Aerodynamics, 98*(10–11), 600–617.
Iaccarino, G., Ooi, A., Durbin, P. A., & Behnia, M. (2003). Reynolds averaged simulation of unsteady separated flow. *International Journal of Heat and Fluid Flow, 24*(2), 147–156.
Janajreh, I., & Simiu, E. (2012). Large eddy simulation of wind loads on a low-rise structure and comparison with wind tunnel results. *Applied Mechanics and Materials, 152–154*, 1806–1813.
Kareem, A., Spence, S. M. J., Bernardini, E., Bobby, S., & Wei, D. (2013). Wind engineering: Using computational fluid dynamics to optimize tall building design. *CTBUH Journal JSTOR, 3*, 38–43.
Kopp, G. A., Mans, C., & Surry, D. (2005). Wind effects of parapets on low buildings: Part 4. Mitigation of corner loads with alternative geometries. *Journal of Wind Engineering and Industrial Aerodynamics, 93*(11), 873–888.
Kopp, G. A., Farquhar, S., & Morrison, M. J. (2012). Aerodynamic mechanisms for wind loads on tilted, roof-mounted, solar arrays. *Journal of Wind Engineering and Industrial Aerodynamics, 111*, 40–52.
Lakehal, D., & Rodi, W. (1997). Calculation of the flow past a surface-mounted cube with two-layer turbulence models. *Journal of Wind Engineering and Industrial Aerodynamics, 67*, 65–78 Elsevier.
Levitan, M. L., & Mehta, K. C. (1992). Texas tech field experiments for wind loads part II: Meteorological instrumentation and terrain parameters. *Journal of Wind Engineering and Industrial Aerodynamics, 43*(1–3), 1577–1588 Elsevier.
Levitan, M. L., Mehta, K. C., Vann, W. P., & Holmes, J. D. (1991). Field measurements of pressures on the Texas Tech building. *Journal of Wind Engineering and Industrial Aerodynamics, 38*(2), 227–234 Elsevier.
Li, C. W., & Yu, L. H. (2010). Hybrid LES/RANS modelling of free surface flow through vegetation. *Computers and Fluids, 39*(9), 1722–1732.
Lin, J. X., Surry, D., & Tieleman, H. W. (1995). The distribution of pressure near roof corners of flat roof low buildings. *Journal of wind Engineering and Industrial Aerodynamics, 56*(2), 235–265 Elsevier.
Lin, J. X., Montpellier, P. R., Tillman, C. W., Riker, W. I., & Gx, H. H. M. (2008). Aerodynamic devices for mitigation of wind damage risk. *The 4th international conference on advances in wind and structures (AWAS'08),* 1533–1546.
Lin, J. X., Montpellier, P. R., & Tillman, C. W. (2011). Aerodynamic edge devices for reduction of wind loads on roofs. *Natural Hazards Review, American Society of Civil Engineers, 24*.
Luo, X. Y., Hinton, J. S., Liew, T. T., & Tan, K. K. (2004). LES modelling of flow in a simple airway model. *Medical Engineering and Physics, 26*(5), 403–413.
Mahmood, M., Srinivas, K., & Budair, M. O. (2008). Experimental study of flow past a low-rise building. *Arabian Journal for Science & Engineering, 33* Springer Science & Business Media BV.
Mehta, K. C., Levitan, M. L., Iverson, R. E., & McDonald, J. R. (1992). Roof corner pressures measured in the field on a low building. *Journal of Wind Engineering and Industrial Aerodynamics, 41*(1–3), 181–192 Elsevier.
Pindado Carrion, S., Meseguer Ruiz, J., Franchini, S. N., & Barrero Gil, A. (2009). *On the reduction of the wind-load on buildings by using cantilever parapets.* Universidad Tecnica de Estambul.
Salaheldin, T. M., Imran, J., & Chaudhry, M. H. (2004). Numerical modeling of three-dimensional flow field around circular piers. *Journal of Hydraulic Engineering, 130*(2), 91–100.
Scanivalve. (2016). ZOC33 Service Manual. Liberty Lake, WA.
Schellenberg, A., Maffei, J., Telleen, K., & Ward, R. (2013). Structural analysis and application of wind loads to solar arrays. *Journal of Wind Engineering and Industrial Aerodynamics, 123*, 261–272.
Shuman, F. (1911). Power from sunshine. *Scientific American, 105*, 291–292.
Shur, M. L., Spalart, P. R., Strelets, M. K., & Travin, A. K. (2008). A hybrid RANS-LES approach with delayed-DES and wall-modelled LES capabilities. *International Journal of Heat and Fluid Flow, 29*(6), 1638–1649.
Singh, G. K. (2013). Solar power generation by PV (photovoltaic) technology: A review. *Energy, 53*, 1–13.
Stathopoulos, T., Baskdran, A., & Go, P. A. (1990). Full-scale measurements of wind pressures on flat roof corners. *Journal of Wind Engineering and Industrial Aerodynamics, 36*, 1063–1072.
Stenabaugh, S. E., Iida, Y., Kopp, G. A., & Karava, P. (2015). Wind loads on photovoltaic arrays mounted parallel to sloped roofs on low-rise buildings. *Journal of Wind Engineering and Industrial Aerodynamics, 139*, 16–26.
Suaris, W., & Irwin, P. (2010). Effect of roof-edge parapets on mitigating extreme roof suctions. *Journal of Wind Engineering and Industrial Aerodynamics, 98*(10–11), 483–491.
Tieleman, H. W., Surry, D., & Lin, J. X. (1994). Characteristics of mean and fluctuating pressure coefficients under corner (delta wing) vortices. *Journal of Wind Engineering and Industrial Aerodynamics, 52*, 263–275 Elsevier.
Troldborg, N., & Sørensen, J. (2014). A simple atmospheric boundary layer model applied to large eddy simulations of wind turbine wakes. *Wind Energy, 17*(April), 657–669.
Tu, J., Yeoh, G.-H., & Liu, C. (2009). *Computational fluid dynamics: A practical approach. Terror and the postcolonial*.
Venkatachari, B. S., Cheng, G. C., Soni, B. K., & Chang, S. C. (2008). Validation and verification of Courant number insensitive CE/SE method for transient viscous flow simulations. *Mathematics and Computers in Simulation, 78*(5–6), 653–670.
Vijiapurapu, S., & Cui, J. (2010). Performance of turbulence models for flows through rough pipes. *Applied Mathematical Modelling, 34*(6), 1458–1466.
Wang, W., Dai, Z., Li, J., & Zhou, L. (2012). A hybrid Laplace transform finite analytic method for solving transport problems with large Peclet and Courant numbers. *Computers and Geosciences, 49*, 182–189.
Webb, S. (2007). Covering the planet with solar panels. *Science, 315*(5813), 869 American Association for the Advancement of Science.
Wegner, B., Maltsev, A., Schneider, C., Sadiki, A., Dreizler, A., & Janicka, J. (2004). Assessment of unsteady RANS in predicting swirl flow instability based on LES and experiments. *International Journal of Heat and Fluid Flow, 25*(3), 528–536.
Zhai, Z. J., Zhang, W., Zhang, Z., & Chen, Q. Y. (2007). Evaluation of various turbulence models in predicting airflow and turbulence in enclosed environments by CFD: Part 1 – Summary of prevalent turbulence models. *Hvac & R Research, 13*(6), 853–870.